Calculation of the circular-polarization P_3 Stokes parameter for electron-silver scattering

Christopher J. Bostock,* Dmitry V. Fursa, and Igor Bray
ARC Centre for Antimatter-Matter Studies, Curtin University, GPO Box U1987, Perth, Western Australia 6845, Australia
(Received 30 October 2013; published 10 December 2013)

We present relativistic convergent close-coupling (RCCC) calculations of the P_3 circular light polarization Stokes parameter for atomic silver associated with the radiative decay of the electron-impact excited $(4d^{10}5p)\ ^2P_{3/2}$ state. The results are compared with the recent measurements of Jhumka *et al*. [Phys. Rev. A **87**, 052714 (2013)]. We find excellent agreement between the RCCC results and experiment across the full energy range of measurements. We also find that relativistic effects have a weak influence on the calculation of P_3 in the energy range considered.

DOI: 10.1103/PhysRevA.88.062707 PACS number(s): 34.80.Dp

I. INTRODUCTION

Electron-superelastic scattering from laser prepared excited states provides a valuable means of performing a "complete" scattering experiment [1,2] where both the magnitude *and* phases of scattering amplitudes can be determined. Recently Jhumka *et al*. [3] have measured the P_3 pseudo-Stokes parameter from the circularly polarized laser excited $(4d^{10}5p)\ ^2P_{3/2}$ state of atomic silver. In the experiment the $(4d^{10}5p)\ ^2P_{3/2}$ state is prepared by a circular-polarized laser excitation of the silver ground state. Electrons are then scattered from this laser prepared state and a superelastic signal (deexcitation to the ground state) is measured as a function of scattering angle and laser polarization. This experiment is the time reverse process of the electron-impact excitation of the $(4d^{10}5p)\ ^2S_{1/2}$-$(4d^{10}5p)\ ^2P_{3/2}$ transition with a coincidence measurement of the fluorescence photon from the excited state and the scattered electron. The advantage of superelastic scattering experiments is that they yield higher counting statistics than the corresponding coincidence experiments.

For the superelastic scattering experiment, the pseudo-Stokes parameters $P_n^{\rm pseudo}$, $n = 1,2,3$, are defined in terms of the differential cross section of the superelastically detected electrons [4]. For the case of $n = 3$ the relation is

$$P_3^{\rm pseudo} = \frac{\rm dcs(RHC) - dcs(LHC)}{\rm dcs(RHC) + dcs(LHC)}, \qquad (1)$$

where dcs(RHC) [dcs(LHC)] denotes the differential cross section associated with scattering from the RHC (LHC) polarized laser excited state. The pseudo-Stokes parameter is related to the optical Stokes parameter $P_3 = 1/K' P_3^{\rm pseudo}$, where $K' = 1$ for the e-Ag measurements of Jhumka *et al*. [3]. To compare with the measurements, we present relativistic convergent close-coupling (RCCC) P_3 Stokes parameter calculations for the electron-impact excitation of the $(4d^{10}5p)\ ^2S_{1/2}$-$(4d^{10}5p)\ ^2P_{3/2}$ transition in atomic silver. Silver is a relatively heavy target ($Z = 47$) with one valence electron above a [Kr]$4d^{10}$ core, therefore e-Ag scattering is well suited to be modeled by the RCCC method which has been successful in calculating observables for other quasi-one-electron and quasi-two-electron heavy atomic targets.

*c.bostock@curtin.edu.au

II. RCCC METHOD

Comprehensive details of the RCCC method for both quasi-one-electron and quasi-two-electron targets are given in Ref. [5] and only the relevant aspects pertaining to e-Ag scattering will be provided here. The silver atom is modeled as one active valence electron above an inert [Kr]$4d^{10}$ Dirac-Fock core. The [Kr]$4d^{10}$ Dirac-Fock core orbitals are obtained using the GRASP package [6]. For the valence electron, a set of one-electron orbitals is obtained by diagonalization of the Ag quasi-one-electron Dirac-Coulomb Hamiltonian in a relativistic (Sturmian) L-spinor basis [7]. Phenomenological one- and two-electron polarization potentials are used to improve the accuracy of the calculated silver wave functions [8,9]; these allow us to take into account more accurately the effect of closed inert shells on the active electrons. The polarization potential parameters depend on the static dipole polarizability of the inert Ag^+ core, which was chosen as $\alpha_c = 9.0$ [10]. The parameters of the polarization potentials, the fall-off radius $r_c^{\rm pol}$ and $r_c^{\rm diel}$, are adjusted to obtain the best representation of target state energies and optical oscillator strength (OOS). For the Ag^+ core we chose $r_c^{\rm diel} = 3.0$, and l-dependent $r_c^{\rm pol}$ with values 2.56, 2.69, and 3.0 for $l = 0,1,2$, respectively. The energy levels of the first ten states used in the calculations are listed in Table I, and the oscillator strengths for the $5s_{1/2}$-$6p_{1/2}$ and $5s_{1/2}$-$6p_{3/2}$ resonance transitions are listed in Table II. For the neutral silver atom we obtain a static dipole polarizability of $38.4a_0^3$, which is substantially lower than the experimental value of $48.6a_0^3$ [11]. This is an indication of the imperfection in the frozen [Kr]$4d^{10}$ Dirac-Fock inert core model; a large part of the static dipole polarizability comes from inner-core excitations. In the present work we have chosen the polarization potential parameters to obtain the most accurate energy levels and resonance transition oscillator strengths (Table II) possible; this is at the expense of obtaining an accurate value for the static dipole polarizability. We note that in the ten states shown in Table I we do not list $(4d^9 5s)\ ^2D_{5/2}$ (3.65 eV) and $(4d^9 5s)\ ^2D_{3/2}$ (4.30 eV) core excited levels since they are not accounted for in the RCCC model.

Our target model consists of 37 states: 15 bound states and 22 continuum states. We found that adding extra continuum states in the scattering calculations did not change the Stokes parameters in the energy range considered.

For the scattering calculation, the generated target states are used to expand the total wave function of the electron-Ag

TABLE I. Energy levels of the first ten silver states calculated by diagonalizing the target in the RCCC method. Experiment levels listed by NIST [12] are also shown.

Configuration	Term	J	RCCC (eV)	Experiment (eV)
$(4d^{10}5s)$	$^2S_{1/2}$	1/2	0.000	0.000
$(4d^{10}5p)$	$^2P_{1/2}$	1/2	3.625	3.664
$(4d^{10}5p)$	$^2P_{3/2}$	3/2	3.736	3.778
$(4d^{10}6s)$	$^2S_{1/2}$	1/2	5.277	5.276
$(4d^{10}6p)$	$^2P_{1/2}$	1/2	5.989	5.988
$(4d^{10}6p)$	$^2P_{3/2}$	3/2	6.016	6.013
$(4d^{10}5d)$	$^2D_{3/2}$	3/2	6.018	6.043
$(4d^{10}5d)$	$^2D_{5/2}$	5/2	6.021	6.046
$(4d^{10}7s)$	$^2S_{1/2}$	1/2	6.640	6.433
$(4d^{10}7p)$	$^2P_{3/2}$	1/2	6.786	6.700
Ionization limit			7.544	7.543

scattering system and formulate a set of relativistic Lippmann-Schwinger equations for the T matrix elements. In this latter step, the relativistic Lippmann-Schwinger equations for the T matrix elements have the following partial wave form for each total angular momentum J and parity Π of the system,

$$T_{fi}^{\Pi J}(k_f\kappa_f,k_i\kappa_i) = V_{fi}^{\Pi J}(k_f\kappa_f,k_i\kappa_i) + \sum_n \sum_\kappa \int dk \frac{V_{fn}^{\Pi J}(k_f\kappa_f,k\kappa)T_{ni}^{\Pi J}(k\kappa,k_i\kappa_i)}{E-\epsilon_n^N-\epsilon_{k'}+i0}. \quad (2)$$

TABLE II. Oscillator strengths of the Ag I ground state compared with experiment [13].

Transition	RCCC	Expt.
$(4d^{10}5p)\ ^2S_{1/2}$-$(4d^{10}5p)\ ^2P_{1/2}$	0.331	0.329
$(4d^{10}5p)\ ^2S_{1/2}$-$(4d^{10}5p)\ ^2P_{3/2}$	0.678	0.707

In Eq. (2), κ denotes the relativistic angular momentum quantum number of the target states ($j = |\kappa| - 1/2$), and the $\sum\!\!\!\!\!\!\int$ symbol denotes the sum over the bound and continuum states of the projectile in the distorting potential of the target. The matrix elements and the method of solution for Eq. (2) using a hybrid OpenMP-MPI parallelization suitable for high-performance supercomputing architectures are given in Ref. [5]. The T matrix elements obtained from the solution of Eq. (2) are used to determine the scattering amplitudes

$$F_{m_fm_i}^{\mu_f\mu_i}(\theta) = -\sum_{\kappa_f\kappa_i J\Pi} i^{L_i-L_f}e^{i\eta_{\kappa_f}+i\eta_{\kappa_i}} C^{jm_j}_{L_fM_f,\frac{1}{2}\mu_f} C^{j'\mu_i}_{L_i0,\frac{1}{2}\mu_i} \times C^{JM_J}_{jm_j,j_fm_f} C^{JM_J}_{j'\mu_i,j_im_i} Y^{M_f}_{L_f}(\boldsymbol{k}_f) \times \sqrt{\frac{2L_i+1}{4\pi}} T_{fi}^{\Pi J}(k_f\kappa_f,k_i\kappa_i) \sqrt{\frac{k_f}{k_i}} \sqrt{\frac{E_fE_i}{c^4}} (2\pi)^2, \quad (3)$$

where $m_j = m_i + \mu_i - m_f$ and $M_f = m_j - \mu_f$.

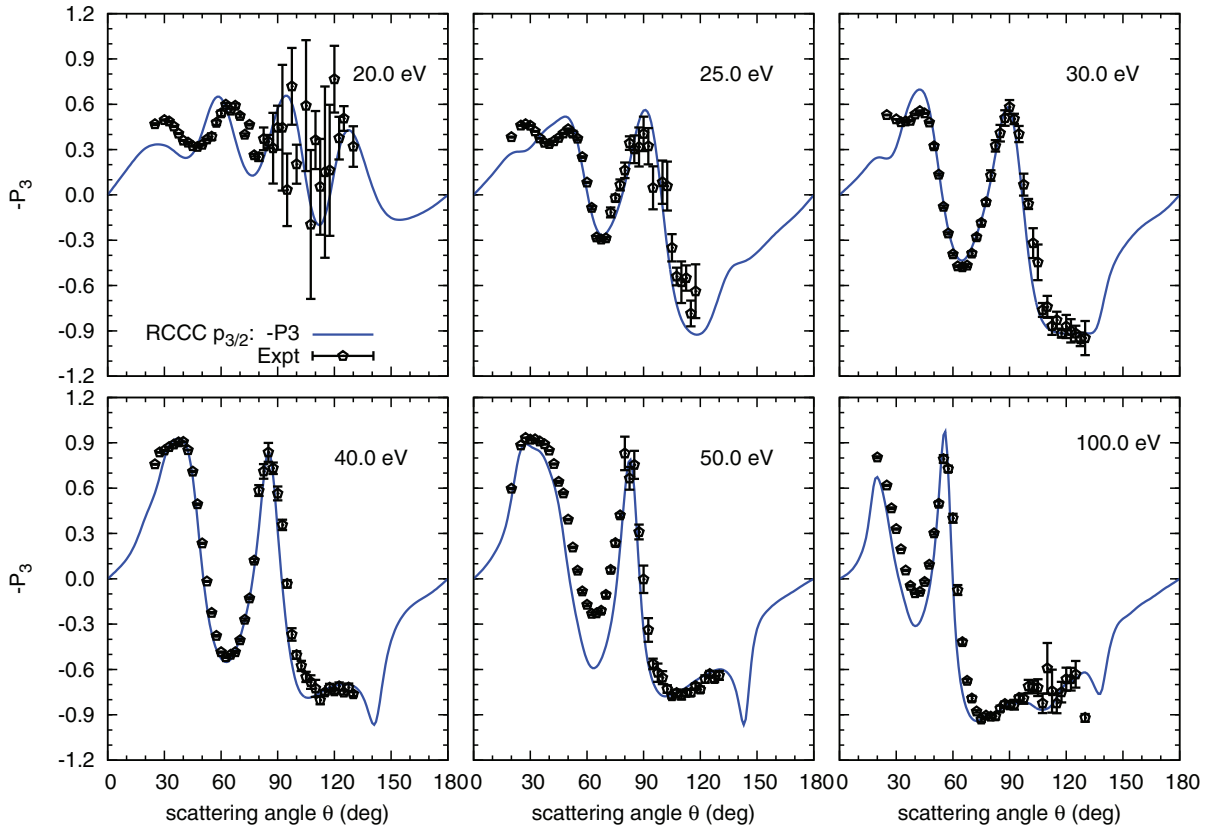

FIG. 1. (Color online) 20–100 eV P_3 RCCC results and measurements of Jhumka *et al.* [3].

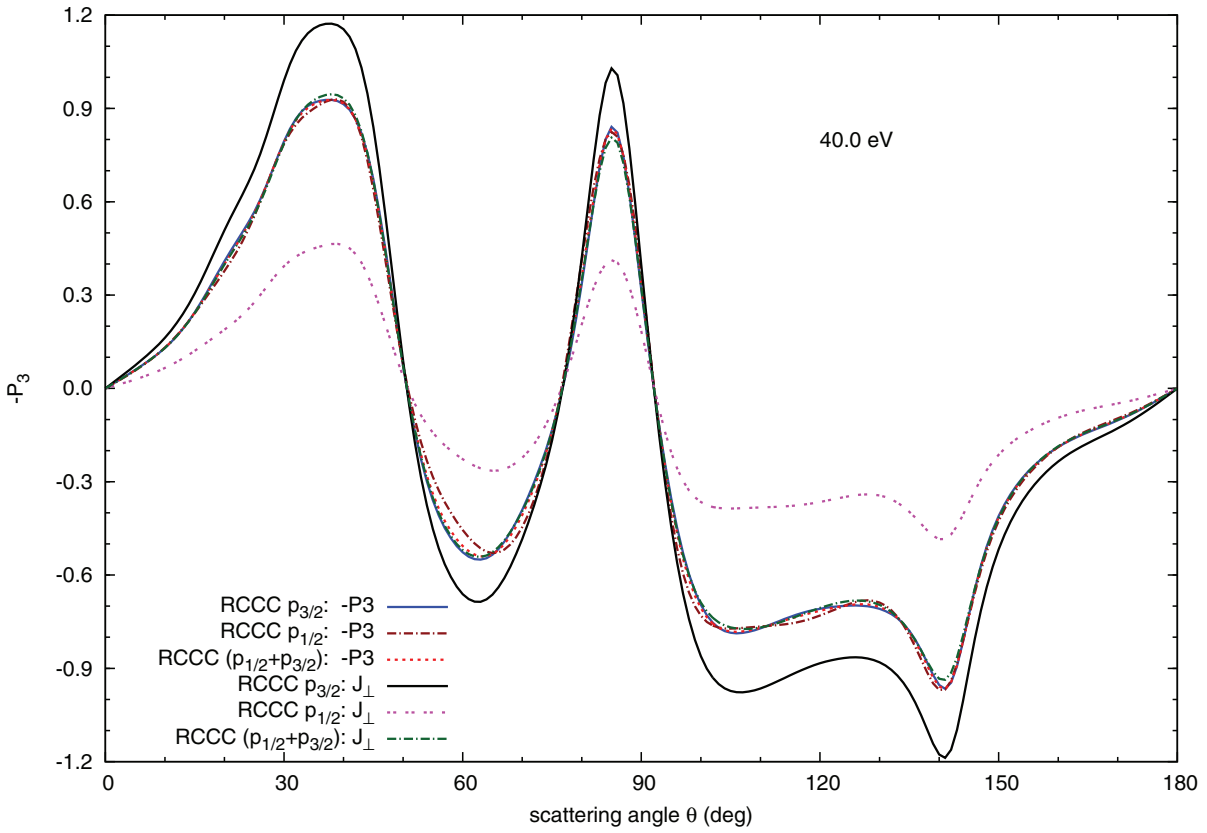

FIG. 2. (Color online) P_3 and $J_\perp$ RCCC results for the $P_{1/2}$, $P_{3/2}$, and combined $P_{1/2} + P_{3/2}$ states at 40 eV.

The scattering amplitudes in turn are used to calculate observables of interest. The details of calculating the P_3 Stokes parameter (circular light polarization) from the scattering amplitudes are described in the Appendix.

III. RESULTS

In Fig. 1 a comparison is made between the RCCC calculations and measurements of Jhumka *et al.* [3] for the $(4d^{10}5p)\ ^2S_{1/2}$-$4(d^{10}5p)\ ^2P_{3/2}$ Stokes parameter P_3. In general, there is excellent agreement between the RCCC calculations and measurements across the full range of energies. Slight discrepancies between theory and the measurements exist: The RCCC result at 50 eV at an angle of 60° is lower than the measurements, and similarly at 100 eV near 30°. Such discrepancies could be a limitation of the frozen [Kr]$4d^{10}$ Dirac-Fock inert core model employed in the scattering calculations. In general, however, at all energies, there is a very good mapping between theory and experiment in the oscillations in P_3 as a function of angle.

In their recent presentation of measurements, Jhumka *et al.* [3] indicated that $L_\perp = -P_3$, where $L_\perp$ is the angular momentum transferred to the target during the collision. This relation, however, strictly only holds in the nonrelativistic case for an s-p transition [14]. To illustrate this point, in Fig. 2 we compare $-P_3$ and $J_\perp$ for the $P_{1/2}$, $P_{3/2}$, and combined $P_{1/2} + P_{3/2}$ states at one energy, 40 eV. The evaluation of the Stokes parameters from the scattering amplitudes, Eq. (3), for the fine-structure resolved and unresolved cases are presented in the Appendix. Two important features are apparent. First, P_3 is nearly identical for the fine-structure resolved $P_{1/2}$ and $P_{3/2}$ states, indicating that relativistic effects are not significant for the Stokes parameter observable in this case. Second, it is only for the combined state $P_{1/2} + P_{3/2}$ calculation that the relation $J_\perp = -P_3$ holds with good accuracy. Note that the last relation reduces to $L_\perp = -P_3$ only in the nonrelativistic limit. The close agreement found between $J_\perp$ and $-P_3$ for the combined feature is another indication of the weak influence of relativistic effects.

In Fig. 3 we compare $-P_3$ and $J_\perp$ across the full range of energies for the $P_{3/2}$ state and combined $P_{1/2} + P_{3/2}$ states across the full range of energies measured. It is apparent that for the $P_{3/2}$ state $J_\perp \neq -P_3$, whereas for the case of combined states the equality holds.

IV. CONCLUSION

We find that RCCC calculations for the P_3 Stokes parameter for electron-impact excitation of the $4d^{10}5p\ ^2S_{1/2}$-$4d^{10}5p\ ^2P_{3/2}$ transition in silver are in excellent agreement with the recent measurements of Jhumka *et al.* [3]. Numerical investigations further indicate that the P_3 results for the $P_{1/2}$ and $P_{3/2}$ states are nearly identical across the range of energies measured, which indicates that relativistic effects are not significant for the P_3 observable in this energy regime. Furthermore, we have shown that for the $P_{3/2}$ state $J_\perp \neq -P_3$, whereas for the case of combined $P_{1/2} + P_{3/2}$ states the relation $J_\perp = -P_3$ holds with good accuracy.

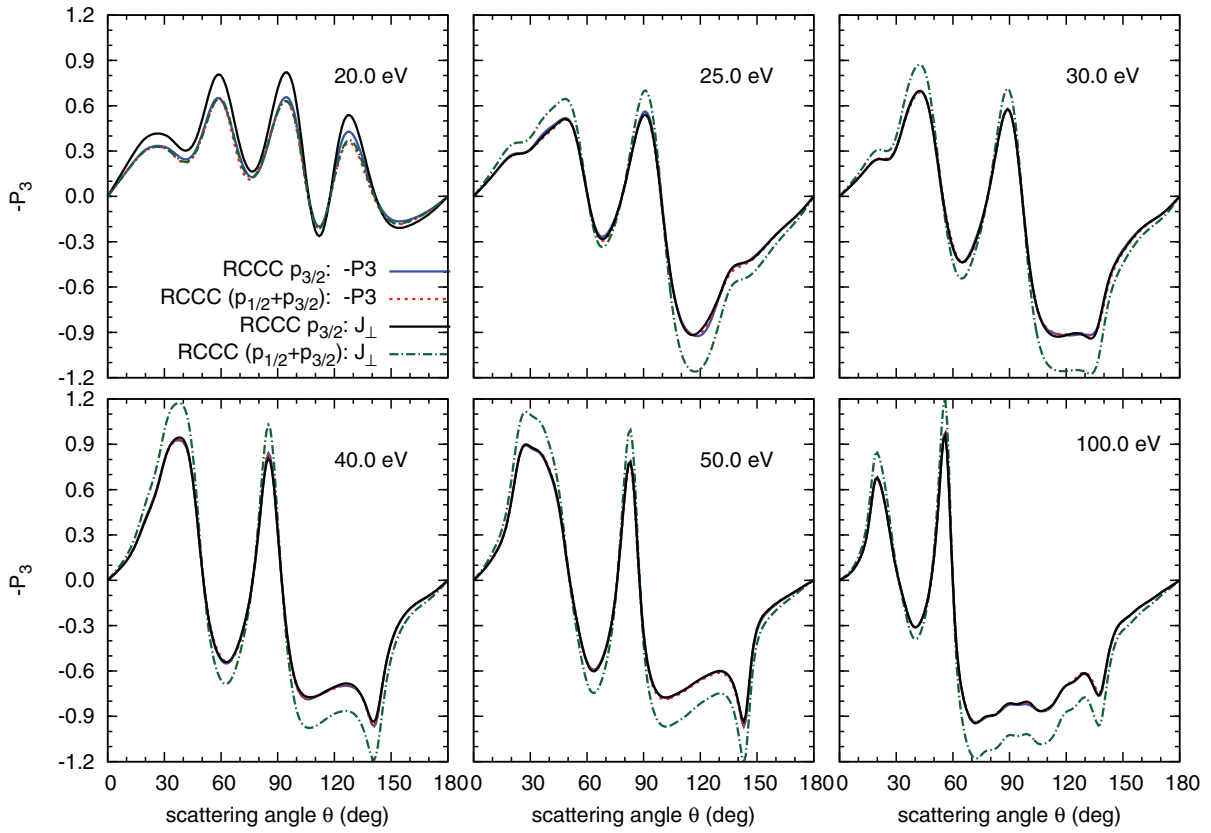

FIG. 3. (Color online) 20–100 eV P_3 and $J_\perp$ RCCC results for the $P_{3/2}$ state, and combined $P_{1/2} + P_{3/2}$ case.

ACKNOWLEDGMENTS

Support of the Australian Research Council and Curtin University is gratefully acknowledged. Calculations were performed on the Australian National Computational Infrastructure facility.

APPENDIX: CALCULATION OF P_3

The calculation of P_3 from the scattering amplitudes is facilitated with the aid of the density matrix formalism [15,16]. The density matrix of the photon emitted in the direction $\{\theta,\phi\}$ during an electric dipole ($E1$) transition from an atomic state with angular momentum J (and other quantum numbers denoted by α) to an atomic state with angular momentum J_f is given by

$$\begin{aligned}\langle\{\theta,\phi\}\lambda|\rho|\{\theta,\phi\}\lambda'\rangle_{\alpha_f J_f} &= \frac{1}{8\pi}|\langle\alpha J_f||D||\alpha J\rangle|^2(2J+1)^{-1/2}\rho_{00}(\alpha J)\\ &\times\left[\delta_{\lambda\lambda'}+\sqrt{6}\sum_{k=1,2}\sum_q \alpha_k^\gamma C^{kq}_{1\lambda,1-\lambda'}\right.\\ &\left.\times\sum_{q'}\mathcal{A}_{kq'}(\alpha J)D^{k*}_{q'q}(\phi,\theta,\psi)\right],\end{aligned} \tag{A1}$$

where $\lambda = \pm 1$ denotes the helicity of the photon, and $\langle\alpha J_f||D||\alpha J\rangle$ denotes the reduced dipole matrix element for the radiative transition. The reduced statistical tensors associated with the electron-atom scattering system are given by

$$\mathcal{A}_{kq} = \frac{\rho_{kq}(j,j)}{\rho_{00}(j,j)}, \tag{A2}$$

where the statistical tensors (state multipoles) are given in terms of the density matrix for the electron-atom collision complex,

$$\rho_{kq}(j,j') = \sum_{mm'}(-1)^{j'-m'}\langle jm,j'-m'|kq\rangle\langle jm|\rho|j'm'\rangle, \tag{A3}$$

with the density matrix given in terms of the scattering amplitudes,

$$\langle jm|\rho|jm'\rangle = \frac{1}{2(2J_i+1)}\sum_{\mu_f\mu_i m_i} F^{\mu_f\mu_i}_{mm_i}(\theta)F^{\mu_f\mu_i}_{m'm_i}(\theta)^*. \tag{A4}$$

In Eq. (A1) the intrinsic anisotropy parameters are given by

$$\alpha_k^\gamma = \sqrt{\frac{3}{2}}\sqrt{2J+1}(-1)^{J+J_f+k+1}\begin{Bmatrix} J & J & k\\ 1 & 1 & J_f\end{Bmatrix}. \tag{A5}$$

We connect the collision frame with the photon frame ("natural frame") via the Wigner rotation matrix $D^{k*}_{q'q}(\phi,\theta,\psi)$ with $\phi = \theta = \pi/2$ and we take $\psi = 0$ for the case of circular polarization.

If fine-structure levels are not resolved, then the density matrix is given by

$$\langle\{\theta,\phi\}\lambda|\rho|\{\theta,\phi\}\lambda'\rangle = \sum_{\alpha_f J_f}\langle\{\theta,\phi\}\lambda|\rho|\{\theta,\phi\}\lambda'\rangle_{\alpha_f J_f}. \quad \text{(A6)}$$

The Stokes parameter P_3 for excitation to a resolved fine-structure level is

$$P_3 = \frac{\langle\lambda=+1|\rho|\lambda'=+1\rangle_{\alpha_f J_f} - \langle\lambda=-1|\rho|\lambda'=-1\rangle_{\alpha_f J_f}}{\langle\lambda=+1|\rho|\lambda'=+1\rangle_{\alpha_f J_f} + \langle\lambda=-1|\rho|\lambda'=-1\rangle_{\alpha_f J_f}}, \quad \text{(A7)}$$

and P_3 for an unresolved fine-structure level is given by the same expression with the replacement of the density matrix given by Eq. (A6).

The angular momentum transferred during the collision can be determined from the statistical tensors [16],

$$\langle J_\perp\rangle = -\sqrt{\frac{2}{3}J(J+1)(2J+1)}\,\mathrm{Im}\left\{\rho_{11}(J,J)\right\}, \quad \text{(A8)}$$

where Im{} denotes the imaginary part.

[1] B. Bederson, Comments At. Mol. Phys. **1**, 41 (1969).
[2] B. Bederson, Comments At. Mol. Phys. **1**, 65 (1969).
[3] S. Jhumka, K. L. Nixon, M. Hussey, and A. J. Murray, Phys. Rev. A **87**, 052714 (2013).
[4] P. M. Farrell, W. R. MacGillivray, and M. C. Standage, Phys. Rev. A **44**, 1828 (1991).
[5] C. J. Bostock, J. Phys. B **44**, 083001 (2011).
[6] K. G. Dyall, I. P. Grant, C. T. Johnson, F. P. Parpia, and E. P. Plummer, Comput. Phys. Commun. **55**, 425 (1989).
[7] I. P. Grant and H. M. Quiney, Phys. Rev. A **62**, 022508 (2000).
[8] D. V. Fursa and I. Bray, J. Phys. B **30**, 5895 (1997).
[9] D. V. Fursa, I. Bray, and G. Lister, J. Phys. B **36**, 4255 (2003).
[10] J. Mitroy, M. S. Safronova, and C. W. Clark, J. Phys. B **43**, 202001 (2010).
[11] J. R. Fuhr and W. L. Wiese, *CRC Handbook of Chemistry and Physics*, 86th ed. (CRC Press, Boca Raton, FL, 2005).
[12] http://physics.nist.gov/PhysRefData/ASD/levels_form.html.
[13] J. Carlsson, P. Jon, and L. Sturesson, Z. Phys. D: At., Mol. Clusters **16**, 87 (1990).
[14] I. V. Hertel and W. Stoll, Adv. At. Mol. Phys. **13**, 113 (1978).
[15] V. Balashov, A. Grum-Grzhimailo, and N. Kabachnik, *Polarization and Correlation Phenomena in Atomic Collisions: A Practical Theory Course* (Springer, New York, 2000).
[16] K. Blum, *Density Matrix Theory and Applications* (Plenum, New York, 1981).